

Towards Performance-Enhanced Model-Contrastive Federated Learning using Historical Information in Heterogeneous Scenarios

Hongliang Zhang, Jiguo Yu, Guijuan Wang, Wenshuo Ma, Tianqing He, Baobao Chai, Chunqiang Hu

Abstract—Federated Learning (FL) enables multiple nodes to collaboratively train a model without sharing raw data. However, FL systems are usually deployed in heterogeneous scenarios, where nodes differ in both data distributions and participation frequencies, which undermines the FL performance. To tackle the above issue, this paper proposes PMFL, a performance-enhanced model-contrastive federated learning framework using historical training information. Specifically, on the node side, we design a novel model-contrastive term into the node optimization objective by incorporating historical local models to capture stable contrastive points, thereby improving the consistency of model updates in heterogeneous data distributions. On the server side, we utilize the cumulative participation count of each node to adaptively adjust its aggregation weight, thereby correcting the bias in the global objective caused by different node participation frequencies. Furthermore, the updated global model incorporates historical global models to reduce its fluctuations in performance between adjacent rounds. Extensive experiments demonstrate that PMFL achieves superior performance compared with existing FL methods in heterogeneous scenarios.

Index Terms—Federated learning, heterogeneous scenarios, model-contrastive, aggregation weight.

I. INTRODUCTION

Federated Learning [1] (FL) is a distributed paradigm that enables multiple nodes to collaboratively train a high-accuracy global model. Since the data originates from edge nodes, it inherently exhibits Non-Independent and Identically Distributed (Non-IID) nature, thereby leading to data heterogeneity in FL [2] [3]. The data heterogeneity causes inconsistent model updates across nodes, significantly degrading the

This work was partially supported by the Major Program of Shandong Provincial Natural Science Foundation for the Fundamental Research under Grant ZR2022ZD03, NSF of China under Grants 62272256, 62202250, and 62372092, the Natural Science Foundation of Sichuan Province under Grant 2025ZNSFSC0512, the Colleges and Universities 20 Terms Foundation of Jinan City under Grant 202228093, and the Shandong Province Youth Innovation Team Project under Grant 2024KJH032. (Corresponding author: Jiguo Yu.)

H. Zhang, G. Wang, and W. Ma are with the Key Laboratory of Computing Power Network and Information Security, Ministry of Education, Shandong Computer Science Center, Qilu University of Technology (Shandong Academy of Sciences), Jinan, 250353, China, Email: hongliangzhang2022@163.com, guijuan_wang@126.com, weimws@foxmail.com.

J. Yu and T. He are with the School of Information and Software Engineering, University of Electronic Science and Technology of China, Chengdu, 610054, China, Email: nstlxfh@gmail.com; jiguoYu@sina.com, sunny.he@std.uestc.edu.cn.

B. Chai is with the School of Computer Science and Engineering, Shandong University of Science and Technology, Jinan, 266590, China, Email: bbchai_915@sdust.edu.cn.

C. Hu is with the School of Big Data and Software Engineering, Chongqing University, Chongqing, 400044, China, Email: chu@cqu.edu.cn.

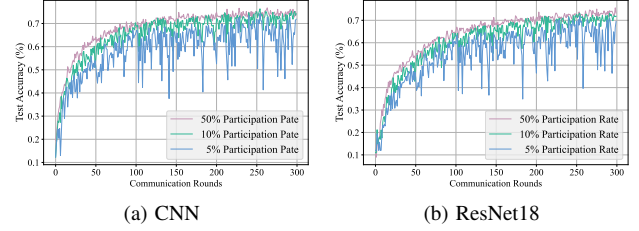


Fig. 1. Test accuracy of global model in FL under varying participation rates on CIFAR10 [11] using average aggregation in the Non-IID setting. Results are shown for two model architectures: (a) CNN and (b) ResNet18.

global model’s performance. Besides, existing studies observe that FL is prone to participation heterogeneity due to the distributed deployment of nodes [4]–[6]. Specifically, it is common in FL to select a subset of nodes to participate in each round of local training (i.e., partial participation) [7] [8]. However, due to higher-priority tasks or unexpected failures, some selected nodes may drop out in certain rounds. This leads to different actual participation frequencies across nodes, known as participation heterogeneity [9] [10]. The study in [4] proves that participation heterogeneity biases the global model toward the local objectives of frequently participating nodes, thereby making the aggregated global model dominated by these nodes. Notably, in practice, FL is inevitably deployed in heterogeneous scenarios where both data heterogeneity and participation heterogeneity coexist, posing significant challenges for designing effective FL algorithms. However, current FL studies focus on only one type of heterogeneity, lacking the ability to tackle both data and participation heterogeneity.

To tackle data heterogeneity, numerous works [12]–[17] have proposed model-contrastive FL methods, which incorporate contrastive learning [18] into the FL optimization. Specifically, these works [12]–[17] maximize the similarity between the representation extracted by the current local model and the positive sample (i.e., the representation extracted by the global model) while minimizing its similarity to the negative one (i.e., the representation extracted by the previous-round local model) for the same input. This promotes alignment between the local and global models, improving the consistency of model updates across nodes under Non-IID data. However, during local iterative optimization, these works [12]–[17] compute the contrastive loss using only a single positive sample and a single negative sample as the contrastive points. This leads to instability of contrastive points across local training process, thereby reducing the effective-

ness of contrastive learning. Moreover, as shown in Fig. 1, we observe that the performance of global model fluctuates sharply between adjacent rounds under partial participation, especially at low participation rates. These fluctuations further exacerbate the instability of contrastive points, making it difficult for the global model to provide stable representations during local training, further weakening contrastive learning’s ability. Meanwhile, participation heterogeneity not only biases the global model toward the local objectives of frequently participating nodes, but also leads to actual participation rates being lower than the preset threshold, further exacerbating fluctuations in the global model’s performance. Therefore, we raise the question: *Is it possible to design an effective model-contrastive FL that tackles the issues caused by data and participation heterogeneity outlined above?*

To answer this question, this paper proposes a **P**erformance-enhanced **M**odel-contrastive **F**ederated **L**earning framework, termed PMFL, which leverages historical information to boost the FL performance under heterogeneous scenarios. The key novelty of PMFL lies in: (i) A novel model-contrastive term is designed in the optimization objective. It incorporates multiple representations from historical local models and employs cosine distance to automatically categorize them to positive and negative samples, thereby constructing stable contrastive points. (ii) The aggregation weight of each node is adaptively adjusted based on its cumulative participation count, to correct the bias in the global objective caused by participation heterogeneity. (iii) The historical global models are incorporated into the global update, thereby reducing fluctuations in global model performance under partial participation.

In summary, our main contributions are four-fold:

- To the best of our knowledge, we are the first to focus on the FL challenges caused by the coexistence of data heterogeneity and participation heterogeneity, and to propose a performance-enhanced model-contrastive FL framework (PMFL) to address the challenges.
- We integrate historical local model information into the model-contrastive term of the node’s optimization function, thereby improving FL performance in Non-IID data.
- We propose an aggregation strategy that adaptively adjusts aggregation weights and incorporates historical global models to alleviate the impact of participation heterogeneity at low participation rates.
- Extensive experiment results on multiple datasets demonstrate that PMFL outperforms various existing methods in diverse heterogeneous scenarios.

The rest of the paper is organized as follows. In Section II, we review related works about FL with heterogeneity. Section III presents the preliminary concepts of FL. Details of the PMFL method are presented in Section IV. The experimental setup and results are shown in Section V and VI, respectively. Finally, Section VII concludes the paper.

II. RELATED WORKS

This section discusses the FL challenges posed by data and participation heterogeneity, and reviews FL works related to contrastive learning.

A. Federated Learning in Data Heterogeneity

Federated learning is a communication-efficient distributed learning paradigm, where multiple nodes submit their model updates without sharing raw training data. However, since each node’s local dataset is not sampled from the global joint distribution, their optimization objectives diverge in direction [19], which significantly degrades the performance of FL. To mitigate the impact of data heterogeneity, numerous solutions can be categorized into two primary types. The first approach focuses on improving the aggregation weight strategy [20]–[23]. For instance, the works in [22] [23] dynamically allocate aggregation weights to nodes by minimizing the convergence rate upper bound. Similarly, the work in [21] proposes a learnable aggregation weight method to adjust each node’s contribution. The second approach is to design regularization objectives to guide local model training in FL [12] [14] [15] [24]–[26]. For instance, the work in [14] incorporates the similarity between the model-level representations into the optimization objective, thereby constraining the optimization direction of local models. Although the aforementioned works enhance the FL performance under data heterogeneity, their effectiveness is limited under participation heterogeneity.

B. Federated Learning in Participation Heterogeneity

Recently, participation heterogeneity has gained attention in FL research. To reduce computation overhead, the classic FedAvg adopts partial participation in each round [1]. However, the work in [5] demonstrates that partial participation leads to performance degradation compared with full participation. To this end, existing works propose various node selection strategies to improve the performance under partial participation [27]–[32]. Their effectiveness relies on the assumption that node participation follows a known probability. In practice, due to node independence and unpredictable failures, the server cannot guarantee that the selected nodes will participate the local training, resulting in heterogeneous participation patterns [33]. Moreover, the work in [4] demonstrates that participation heterogeneity induces bias in the global objective. Specifically, when certain nodes participate more frequently, the learned global model is skewed toward their local objectives, deviating from the true global objective.

To mitigate the negative impact of participation heterogeneity, existing studies [5] [6] incorporate each node’s most recent model update into the current round’s global update, regardless of their participation status. However, because many nodes may remain inactive for extended periods, integrating their outdated updates into the current global update may degrade FL performance. To this end, the work in [4] proposes an adaptive aggregation weight adjustment strategy based on nodes’ historical participation information to address participation heterogeneity. In addition, several FL variants have been proposed to accelerate convergence under participation heterogeneity [34]–[36]. Although these solutions have made progress in tackling participation heterogeneity, the coexistence of data heterogeneity and participation heterogeneity continues to cause performance degradation in FL.

C. Contrastive Learning

Contrastive learning has emerged as a prominent research area, achieving remarkable effectiveness in learning high-quality feature representations from unlabeled data [37] [38]. Its core idea is to minimize the distance between representations of different augmented views of the same sample (positive pairs), while maximizing the distance between representations of augmented views of different samples (negative pairs). A notable study first incorporates contrastive learning into federated learning and proposes a model-contrastive FL, named MOON [12]. Subsequently, the works [14]–[16] are proposed as variations of MOON. For instance, the work in [16] proposes a dense contrastive-based FL that leverages multi-scale representations with dense features to learn more expressive representations. However, these works [13]–[16] use only a single positive sample from the global model and a single negative sample from the previous-round local model as contrastive points, which makes it difficult to capture stable contrastive points across local training. In addition, under participation heterogeneity with low participation rates, the performance of the global model fluctuates sharply across adjacent rounds, thereby exacerbating the instability of contrastive points. Thus, there is a current research gap in addressing the above challenges under heterogeneous scenarios. To bridge this gap, we propose a performance-enhanced model-contrastive FL framework to tackle the above issues.

III. PRELIMINARIES

The FL system usually consists of a server and K nodes. Let \mathcal{K} represent the set of nodes, with the local dataset of node k denoted as \mathcal{D}_k , and the overall dataset given by $\mathcal{D} := \bigcup_{k \in \mathcal{K}} \mathcal{D}_k$. The objective of FL is to learn a global model W on the dataset \mathcal{D} to solve the following optimization problem:

$$W^* = \arg \min_W \frac{1}{K} \sum_{k \in \mathcal{K}} F(\mathcal{D}_k, W), \quad (1)$$

where $F(\mathcal{D}_k, W) := \mathbb{E}_{(x,y) \sim \mathcal{D}_k} [l((x,y), W)]$ represents the local objective of node k , $l(\cdot)$ denotes the (local) empirical risk, and W^* is the optimal global model. In the t -th round, each selected node k trains the received global model W^t on its local data to obtain the updated local model w_k^t . The node then submits its model update $\Delta_k^t := w_k^t - W^t$ to the server. The global model W^t is updated as follows:

$$W^{t+1} = W^t + h(\Delta_1^t, \Delta_2^t, \dots, \Delta_k^t), \quad (2)$$

where $h(\cdot)$ denotes the function used to calculate the global update. However, data heterogeneity leads to inconsistent model updates across nodes, which degrades the FL performance. In addition, participation heterogeneity causes the global model to learn toward the optimization objective of frequently participating nodes. The study in [4] formalizes the relationship between nodes' participation frequency and the global objective, as stated in Theorem 1.

Theorem 1. *Given that the node k participates in each round with probability p_k , and its aggregation weight x_k^t is time-constant, i.e., $x_k^t = x_k$, but generally x_k may not be equal to $x_{k'}$, the FL minimizes the following objective:*

$$W^* = \arg \min_W \frac{1}{Y} \sum_{k \in \mathcal{K}} x_k p_k F(\mathcal{D}_k, W), \quad (3)$$

where $Y = \sum_{k \in \mathcal{K}} x_k p_k$.

Theorem 1 indicates that when all nodes participate with the same frequency (i.e., $p = p_k, \forall k$), FL converges to an objective weighted by x_k , which differs from the objective defined in formula (1). However, if all nodes are assigned the same aggregation weight x_k , the global model becomes inherently biased toward nodes that participate more frequently. Furthermore, in practice, node participation frequencies are typically unknown, making it difficult to define a fixed optimization objective for FL. Thus, it is necessary to design an adaptive strategy to adjust the aggregation weight x_k for minimizing the objective in formula (1) under participation heterogeneity.

IV. THE DESIGN OF PMFL

This section provides a high-level overview of the PMFL framework, followed by a detailed description.

A. High-Level Description of PMFL

The PMFL framework consists of a central server and multiple nodes. The server collaborates with the nodes to perform federated training. In each round, PMFL performs the following three phases.

- *Phase I. Node Selection:* The server randomly selects a subset of nodes for the current round, and distributes the latest global model parameters to the selected nodes.
- *Phase II. Local Model Training:* If a node participates in training, it initializes its local model using the received global model parameters and fine-tunes the model by optimizing the local objective. After completing the training, each participating node sends its model update to server.
- *Phase III. Aggregation:* The server aggregates the submitted model updates to calculate the updated global model.

The process from *Phase I* to *Phase III* is repeated until the predetermined T rounds are completed. Notably, we establish a local sliding buffer at each node to store its historical local models, and a global sliding buffer on the server to store historical global models. During *Local Model Training*, the model-contrastive term incorporates the historical local models stored in the local buffer, thereby forming a novel optimization function. In *Aggregation*, the global model is computed using each node's cumulative participation count and the historical global models stored in the global buffer. The detailed procedures of *Phase I* to *III* are presented below.

B. Node Selection Phase

To reduce computation overhead, the server selects a subset of nodes to participate in training in each round. Since each node independently decides whether to participate based on its availability, some selected nodes may drop out. To formally indicate each node's participation status, we define an indicator \mathbb{A}_k^t , where $\mathbb{A}_k^t = 1$ if node k participates in round t and $\mathbb{A}_k^t = 0$ otherwise. Thus, only nodes with $\mathbb{A}_k^t = 1$ perform the *Local Model Training* phase in t -th round.

Algorithm 1: Local Model Training

Input: $E, \mathcal{D}_k, W^t, \eta_l$. $\triangleright \mathcal{D}_k$ is local dataset of node k , E denotes the number of local iterations, W^t is the global model parameters, η_l is the local learning rate.

Output: $\{\Delta_k^t\}_{k \in \mathcal{K}}$.

```

1  $\{\mathbb{A}_k^t\}_{k \in \mathcal{K}} \leftarrow \{0, 1\}$ ;
2 for each node  $k \in \mathcal{K}$  do
3   if  $\mathbb{A}_k^t = 1$  then
4      $w_k^{tE} \leftarrow W^t$ ;
5     for each iteration  $e \in \{0, \dots, E-1\}$  do
6       Randomly sample  $\mathcal{D}_k^{t,e} \subset \mathcal{D}_k$ ;
7        $g_k^{tE+e} \leftarrow \nabla F(\mathcal{D}_k^{t,e}, w_k^{tE+e})$ ;
8        $w_k^{tE+e+1} \leftarrow w_k^{tE+e} - \eta_l g_k^{tE+e}$ ;
9      $\Delta_k^t \leftarrow w_k^{(t+1)E} - w_k^{tE}$ ;
10  else
11     $\Delta_k^t \leftarrow 0$ ;
12  Send  $\Delta_k^t$  to server;
```

C. Local Model Training Phase

Insights. As shown in Algorithm 1, nodes with $\mathbb{A}_k^t = 1$ fine-tune the global model received from the server. However, data heterogeneity causes the deviations in optimization directions across nodes, degrading the FL performance. Existing FL works [13]–[16] integrate a model-contrastive term into the optimization objective to mitigate the impact of data heterogeneity. These methods rely on a single global representation as the positive sample and a single previous local representation as the negative sample. This leads to instability of contrastive points across local iterations. To this end, we incorporate historical local models into the model-contrastive term to provide additional positive and negative samples, thereby capturing more stable contrastive points. The representations learned by these historical local models are assigned as positive or negative samples based on their similarities from the representation learned by the current local model under the same input. In the following, we first describe the model architecture and then present the optimization function.

1) *Model Architecture:* Each local model, parameterized by w , consists of an encoder layer, a projection layer, and a classification layer, formalized as $\text{Enc}(\cdot, ({}^1w)$, $\text{Pro}(\cdot, ({}^2w)$, and $\text{Cla}(\cdot, ({}^3w)$, respectively. Each layer is parameterized by a distinct subset of w . These subsets satisfy $w = ({}^1w) \cup ({}^2w) \cup ({}^3w)$ and $({}^i w) \cap ({}^{i'}) w = \emptyset$ for all $i \neq i'$.

- **Encoder Layer.** This layer is a neural network, such as a Convolutional Neural Network [39] (CNN) or Residual Network [40] (ResNet), designed to transform input samples into an encoder vector.
- **Projection Layer.** This layer consists of a multi-layer perceptron and an activation function. It maps the encoded vector into a projected representation vector. Given a local model w and sample feature x , the local representation vector is computed as $z = \text{Pro}(\text{Enc}(x, ({}^1w), ({}^2w))$. For simplicity, we express the relation as $z = \text{Pro}(\text{Enc}(x, w), w)$.
- **Classification layer.** The layer takes the representation vector as input and produces class probabilities used to calculate the classification loss.

2) *Optimization Function:* Each node fine-tunes its local model using the designed optimization function. For classification tasks, this function consists of a classification term l_{cro} used for classification, and a model-contrastive term l_{con} designed to align the local models with the global model. The term l_{con} leverages additional positive and negative samples to compute the contrastive loss, as detailed below.

Specifically, each node k maintains a local sliding buffer \mathcal{S}_l of length N that stores its most recent local models. Let E be the number of local iterations per round with $0 \leq e \leq E-1$. The local model of node k at the e -th local iteration of round t is denoted by w_k^{tE+e} . Thus, the local buffer is defined as $\mathcal{S}_l := \{w_k^{tE+e-N}, \dots, w_k^{tE+e-1}\}$. When \mathcal{S}_l is filled, the earliest model is replaced by the newest one. Given a sample feature x , the node computes its historical representation using each model stored in the buffer. Formally, the set of historical local representation vectors is defined as:

$$\mathcal{Z} = \left\{ z_k^j = \text{Pro}(\text{Enc}(x, w_k^j), w_k^j) \mid j \in [tE + e - N, tE + e - 1] \right\}.$$

Based on the set \mathcal{Z} , the node calculates the similarity between each historical local representation vector z_k^j and the current local representation vector z_k^{tE+e} . Given a threshold μ , if the similarity is greater than or equal to μ , the vector z_k^j is regarded as a positive sample and added to the positive sample set \mathcal{Z}^+ . Conversely, z_k^j is allocated to the negative sample set \mathcal{Z}^- . Formally, the sets \mathcal{Z}^+ and \mathcal{Z}^- are defined as:

$$\begin{aligned} \mathcal{Z}^+ &= \left\{ z_k^j \in \mathcal{Z} \mid \text{Sim}(z_k^{tE+e}, z_k^j) \geq \mu \right\}, \\ \mathcal{Z}^- &= \left\{ z_k^j \in \mathcal{Z} \mid \text{Sim}(z_k^{tE+e}, z_k^j) < \mu \right\}, \end{aligned}$$

where $\text{Sim}(a, b) = a^T b / (\|a\| \|b\|)$ represents the cosine similarity between a and b . The similarity value closer to 1 means that the two vectors are aligned in direction, whereas the value closer to -1 indicates they are opposite. The threshold μ is defined to $\text{Sim}(z_k^{tE}, Z^t)$, where Z^t is the global representation derived from the global model W^t . This threshold varies across nodes k in each round. The two sample sets satisfy $\mathcal{Z}^+ \cup \mathcal{Z}^- = \mathcal{Z}$ and $\mathcal{Z}^+ \cap \mathcal{Z}^- = \emptyset$. Notably, at the beginning of each iteration, \mathcal{Z}^+ and \mathcal{Z}^- are reset to empty sets. To construct stable contrastive points, we aim to minimize the distance between z_k^{tE+e} and the representations in $Z^t \cup \mathcal{Z}^+$, while maximizing its distance from the representations in \mathcal{Z}^- . Thus, similar to [12], the model-contrastive loss is defined as:

$$l_{con} = -\log \frac{\text{pos}}{\text{pos} + \text{neg}}, \quad (4)$$

where pos and neg is computed as follows:

$$\begin{aligned} \text{pos} &= \exp \left(\frac{\text{Sim}(z_k^{tE+e}, Z^t)}{\tau} \right) + \sum_{z_k^j \in \mathcal{Z}^+} \exp \left(\frac{\text{Sim}(z_k^{tE+e}, z_k^j)}{\tau} \right), \\ \text{neg} &= \sum_{z_k^j \in \mathcal{Z}^-} \exp \left(\text{Sim}(z_k^{tE+e}, z_k^j) / \tau \right). \end{aligned}$$

Here, τ is the temperature coefficient controlling the scaling of the similarity. Combining the terms l_{cro} and l_{con} , the loss for an input sample (x, y) is given by:

$$\mathcal{L} = l_{cro}((x, y), w_k^{tE+e}) + \lambda l_{con}(x, W^t, \mathcal{S}_l), \quad (5)$$

where l_{cro} is the classification loss, λ is the importance coefficient of model-contrastive term, x is the sample feature, and y is the sample label. Formally, the local objective of node

k is defined as:

$$\min_{w_k} F(\mathcal{D}_k, w_k) = \mathbb{E}_{(x,y) \sim \mathcal{D}_k} \mathcal{L}. \quad (6)$$

3) *Fine-tuned Model*: Nodes with $\mathbb{A}_k^t = 1$ fine-tune their local models using the aforementioned model architecture and optimization objective. During the e -th local iteration, the node k randomly samples a mini-batch $\mathcal{D}_k^{t,e}$ from its local dataset \mathcal{D}_k , and calculates the gradient g_k^{tE+e} based on the optimization function:

$$g_k^{tE+e} = \nabla F(\mathcal{D}_k^{t,e}, w_k^{tE+e}),$$

where ∇ denotes the derivative operation. The local model is then updated via stochastic gradient descent:

$$w_k^{tE+e+1} = w_k^{tE+e} - \eta_l g_k^{tE+e},$$

where η_l is the local learning rate. After completing E local iterations, the node calculates its model update as follows:

$$\Delta_k^t = w_k^{(t+1)E} - w_k^{tE},$$

and submits Δ_k^t to the server. Notably, for nodes with $\mathbb{A}_k^t = 0$, the model update Δ_k^t is set to zero vector.

D. Aggregation Phase

We propose an aggregation strategy consisting of the *Adaptive Aggregation Weight Calculation* step and the *Global Model Aggregation* step. First, the server adjusts each node's aggregation weight based on its cumulative participation count to mitigate the bias caused by participation heterogeneity. Second, the server incorporates historical global models into the global update to reduce performance fluctuations.

1) *Adaptive Aggregation Weight Calculation*: **Insights.** The global optimization objective defined in formula (3) is equivalent to that in formula (1) when the aggregation weight x_k is set to $1/p_k$ for each node k under participation heterogeneity. Given T rounds, the relation $x_k = 1/p_k$ can be rewritten as:

$$x_k = 1/p_k = 1/\frac{M_k}{T} = T/M_k, \quad (7)$$

where M_k denotes the cumulative participation count of node k over T rounds. Formula (7) shows that the weight x_k equals T/M_k , which is interpreted as the average participation interval of node k when the first interval starts at round $t=0$. However, since a node's future participation status is unknown, M_k is not available a priori. Thus, in the t -th round, the weight x_k can be estimated using the current cumulative participation count of node k . Nevertheless, this estimation method faces two issues. (i) If a node has not participated in any previous rounds, its average interval cannot be estimated. (ii) When the current round t is small and node k has participated frequently, the estimated average interval may deviate from the ideal optimal value T/M_k . To this end, we introduce a positive integer $C \in \mathbb{N}^+$ as the "cutoff" interval. Specifically, if node k has not participated in any of the most recent C rounds, its cumulative participation count is incremented by 1. Using the cutoff interval C to calculate the average participation interval effectively mitigates the above issues. Notably, when C is too large, it is difficult to estimate the average interval if a node has not participated for many rounds. In contrast, a smaller C may overestimate the node's actual participation frequency. Thus, selecting an appropriate C value can effectively improve the FL performance, as validated by our experimental results.

Algorithm 2: Aggregation

Input: $C, \eta_g, H, \mathbb{A}_k^t, \Delta_k^t, Q_k, R_k$. $\triangleright C$ is cutoff interval, η_g is the global learning rate, H is the size of global sliding buffer, Δ_k^t is the model update of node k , Q_k is the current participation interval of node k , and R_k is the current participation count of node k .

Output: W^{t+1} .

```

1 // Adaptive Aggregation Weight Calculation
2 for each node  $k \in \mathcal{K}$  do
3    $Q_k \leftarrow Q_k + 1$ ;
4   if  $\mathbb{A}_k^t = 1$  or  $Q_k = C$  then
5      $Q_k^* \leftarrow Q_k$ ;
6     if  $R_k = 0$  then
7        $x_k^t \leftarrow Q_k^*$ ;
8     else
9        $x_k^t \leftarrow (R_k \cdot x_k^{t-1} + Q_k^*) / (R_k + 1)$ ;
10     $R_k \leftarrow R_k + 1$ ;  $Q_k \leftarrow 0$ ;
11  else
12     $x_k^t \leftarrow x_k^{t-1}$ ;
13 // Global Model Aggregation
14  $W^{t+1} =$ 
15    $(1 - \psi) (W^t - \eta_g \sum_{k \in \mathcal{K}} x_k^t \Delta_k^t) + \frac{\psi}{H-1} \sum_{h=1}^{H-1} W^{t-h}$ ;
16 Distribute the global model  $W^{t+1}$  to nodes ;

```

Based on the above insights, the server calculates each node's aggregation weight using its cumulative participation count, as shown in Algorithm 2. Let R_k denote the current participation count (including cutoffs) of node k , and let Q_k denote its current participation interval, i.e., the number of rounds elapsed since its last participation. At the beginning of the FL task, both Q_k and R_k are initialized to 0. Specifically, in the aggregation phase, the server increments the current participation interval Q_k by 1 for each node. If node k satisfies $\mathbb{A}_k^t=1$ or $Q_k=C$, its aggregation weight is updated based on its current average participation interval. In contrast, for other nodes, the aggregation weight remains unchanged. For nodes whose weights need to be updated, their current participation interval Q_k is recorded as Q_k^* . If such a node has never participated in the previous $(t-1)$ rounds (including cutoff), its aggregation weight is set as $x_k^t \leftarrow Q_k^*$. Conversely, the aggregation weight of node k is updated as:

$$x_k^t = (R_k \cdot x_k^{t-1} + Q_k^*) / (R_k + 1), \quad (8)$$

where x_k^t is interpreted as the average participation interval of node k up to round t . After the weight x_k^t is updated, the current participation count R_k is incremented by 1 only for nodes satisfying $\mathbb{A}_k^t=1$ or $Q_k=C$, and the current interval Q_k is reset to 0. Notably, the server can obtain each node's aggregation weight regardless of whether the node participates in the current round.

2) *Global Model Aggregation*: To compute the updated global model W^{t+1} , the server uses the aggregation weight x_k^t to determine each node's contribution. Formally, the global model is updated as follows:

$$W^{t+1} = W^t - \eta_g \sum_{k \in \mathcal{K}} x_k^t \Delta_k^t, \quad (9)$$

where η_g is the global learning rate. Notably, nodes that do not participate in the current round have $\Delta_k^t=0$. Thus, they do not influence the aggregation results. Although adjusting the

aggregation weights mitigates the global model bias caused by participation heterogeneity, the global model performance may fluctuate when the participation rate is low, as shown in Fig. 1 of Section I. This fluctuation weakens the global representation extracted by the global model in the model-contrastive term.

To alleviate performance fluctuations of the global model, we incorporate historical global models into the updated global model. Specifically, the server maintains a global sliding buffer \mathcal{S}_g that stores the most recent H global models, thereby preserving historical information from previous rounds. Formally, the update rule of the global model is rewritten as:

$$W^{t+1} = (1 - \psi) (W^t - \eta_g \sum_{k \in \mathcal{K}} x_k^t \Delta_k^t) + \frac{\psi}{H-1} \sum_{h=1}^{H-1} W^{t-h}, \quad (10)$$

where ψ is a dynamic coefficient defined by:

$$\psi = 1/2 - t/(2(T - 1)). \quad (11)$$

As the number of rounds increases, the global model gradually converges. Thus, the dynamic coefficient ψ can progressively reduce the reliance of the updated global model W^{t+1} on historical global models. By this step, the server obtains the updated global model W^{t+1} for the current round.

V. EXPERIMENTAL SETUP

This section presents the experimental datasets and model structures, the settings for heterogeneity, and provides a detailed hyper-parameter settings and compared methods.

A. Datasets and Model Structures

In our evaluation, we validate PMFL on multiple datasets, including SVHN, CIFAR10, CINIC, and CIFAR100. All nodes adopt the same model architecture within each dataset.

- For SVHN [41] dataset, the model consists of two convolutional layers used as the encoder and two fully connected layers used as the classifier.
- For CIFAR10 [11] dataset, the model includes two convolutional layers used as the encoder and three fully connected layers as the classifier.
- For CIFAR100 [11] and CINIC [42] datasets, the model consists of two convolutional layers used as the encoder and three fully connected layers as the classifier.

Each convolutional layer employs a kernel size of 3×3 , followed by a Rectified Linear Unit (ReLU) function and a max-pooling layer with a kernel size of 2×2 .

B. Heterogeneity Settings

To simulate data heterogeneity, we follow the existing FL works [43] [44] and employ a Dirichlet distribution [45] with concentration parameter α to generate the class distribution for each node, thereby constructing the Non-IID setting. The parameter α controls the degree of data heterogeneity, with a smaller α indicating the higher degree of data heterogeneity. In addition, to simulate participation heterogeneity, we generate each node's actual participation frequency using a Dirichlet distribution with parameter β . A smaller β indicates the larger difference in participation frequencies among nodes.

More specifically, to generate each node's participation probability, a vector \mathbf{Z} is sampled from the Dirichlet distribution with parameter β , where the dimension of \mathbf{Z} is the

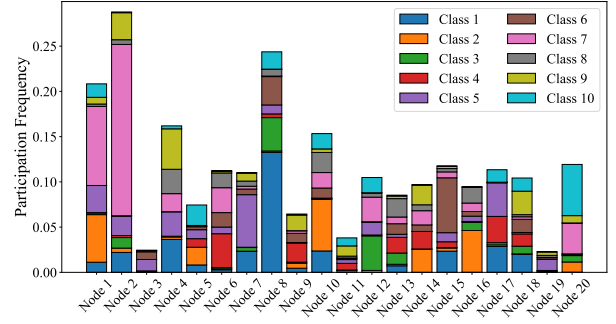


Fig. 2. Visualization of class distributions and participation frequencies across 20 nodes.

same as that of each node's class distribution vector \mathbf{D}_k . The participation frequency of node k is then calculated as:

$$p_k = \begin{cases} \frac{\langle \mathbf{Z}, \mathbf{D}_k \rangle}{r}, & \text{if } \frac{\langle \mathbf{Z}, \mathbf{D}_k \rangle}{r} \geq 0.02, \\ 0.02, & \text{otherwise.} \end{cases} \quad (12)$$

where $\langle \cdot, \cdot \rangle$ denotes the inner product, and r is the normalization factor that ensures $\mathbb{E}[p_k] = 0.1$, thereby simulating a low participation rate in FL. The minimum participation frequency is capped at 0.02. For example, in a 10-class classification task, the vectors \mathbf{D}_k and \mathbf{Z} are sampled independently from Dirichlet distributions with parameters $\alpha=0.1$ and $\beta=0.1$, respectively. Assuming the vector \mathbf{Z} is given by:

$$\mathbf{Z} = [0.38, 0.10, 0.01, 0.00, 0.00, 0.01, 0.44, 0.04, 0.03, 0.00],$$

the participation frequency p_k is calculated using formula (12). Since $\mathbf{Z}[7] = 0.44$ is the maximum value, nodes with a higher proportion of class-7 samples tend to have higher participation frequencies. Fig. 2 visualizes the relationship between data heterogeneity and participation heterogeneity.

Although the Dirichlet distribution determines each node's participation frequency, it does not capture the temporal dynamics of participation. To address this, we introduce distinct participation patterns in our experiments, namely bernoulli, markovian, and cyclic, to simulate unknown participation states of each node. Fig. 3 visualizes the three participation patterns. The details of these patterns are specified as follows.

- In bernoulli pattern, each node determines its participation status at each round based on a bernoulli distribution parameterized by p_k . Formally, the participation status $\mathbb{A}_k^t \in \{0, 1\}$ is given by:

$$P(\mathbb{A}_k^t = 1) = p_k, \quad P(\mathbb{A}_k^t = 0) = 1 - p_k,$$

where $P(\mathbb{A}_k^t = 1)$ denotes the probability that the node participates in each round. Since the participation status across rounds is independent, we have $P(\mathbb{A}_k^t | \mathbb{A}_k^{t-1}) = P(\mathbb{A}_k^t)$, ensuring that the participation status exhibits no temporal dependency.

- In markovian pattern, each node switches between participation and non-participation based on a two-state Markov chain. The transition probabilities are defined by:
 - $p_k^{0 \rightarrow 1}$: Transition probability from non-participation to participation, set by default to 0.05.
 - $p_k^{1 \rightarrow 0}$: Transition probability from participation to non-participation, derived as:

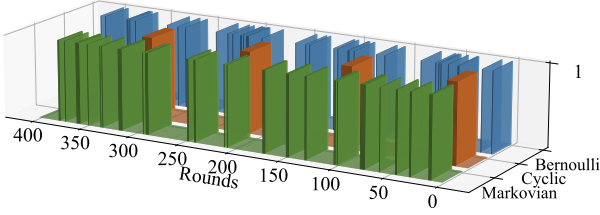


Fig. 3. Visualization of various participation patterns $\mathbb{E}[p_k] = 0.1$ over the first 400 Rounds for a single node.

$$p_k^{1 \rightarrow 0} = (1 - p_k) \cdot p_k^{0 \rightarrow 1}.$$

The transition probabilities ensure that the node’s participation frequency remains stable in subsequent rounds.

- In cyclic pattern, each node alternates between participation and non-participation within a fixed-length cycle of T_{cycle} rounds. Specifically, node k participates in training for $p_k \times T_{cycle}$ rounds per cycle, and does not participate for the remaining $(1 - p_k) \times T_{cycle}$ rounds. To simulate the diversity of node participation, each node begins its cycle with a random offset $o_k \in [0, T_{cycle})$. The participation status \mathbb{A}_k^t at round t is formally defined as:

$$\mathbb{A}_k^t = \begin{cases} 1, & \text{if } (t - o_k) \bmod T_{cycle} < p_k \times T_{cycle}, \\ 0, & \text{otherwise.} \end{cases}$$

We set the cycle length to 100 rounds. This pattern combines periodic and random elements, capturing the participation dynamic in real-world scenarios.

C. Hyper-Parameter Setting

The experiments simulate 250 nodes, each configured with the identical hyper-parameters. Unless otherwise specified, the following default settings are adopted. The local learning rate η_l is set to 0.1, the global learning rate η_g to 1, and the temperature parameter τ to 0.5. The number of local iterations E is 5. The importance coefficient of model-contrastive term λ is 0.5. The global buffer size H is 3, and local buffer size N is 5. The “cutoff” interval length C is set to 50. To simulate data heterogeneity and participation heterogeneity, the Dirichlet parameters α and β are both set to 0.1. To simulate a scenario with low participation rate, the expected participation frequency is set to $\mathbb{E}[p_k]=0.1$, which means that on average only 25 nodes participate in each round. The number of rounds T is set to 1000 for SVHN, 10000 for CIFAR10, CINIC, and CIFAR100.

D. Compared Methods

We compare our PMFL with several baseline methods. FedVarp [5] and MIFA [6]: Both methods maintain and reuse the most recent update from each node, and aggregate these cached updates during the aggregation phase to approximate the current global update. FedHyper [46]: The method is a hyper-gradient-based learning-rate scheduling algorithm for FL that adopts average aggregation. FedAU [4]: This method assigns aggregation weights to model updates during aggregation based on each node’s average participation interval.

FedPPO [30]: The method evaluates each node’s contribution by combining the accuracies of the global and local models, and selects high-contribution nodes for the next round.

VI. EXPERIMENTAL RESULTS

This section reports and analyzes the performance of PMFL in heterogeneous scenarios.

1) *Performance of PMFL and Compared Methods:* The accuracy of PMFL and the baseline methods is evaluated on SVHN, CIFAR10, CINIC, and CIFAR100. All hyper-parameters are set to their default values. The results are reported in Table I. For each column, the best-performing result in each sub-table is highlighted in bold. Each result in the table is obtained by calculating the average of the top-5 accuracy values from the corresponding experimental runs. It can be observed that PMFL achieves higher accuracy than other methods under different participation patterns. This superior performance is attributed to the following three key factors. First, PMFL incorporates historical global models into the computation of the current global model during aggregation, thereby mitigating the performance fluctuations caused by low participation rates. Second, it dynamically adjusts the aggregation weights based on each node’s current participation count, enabling the global optimization objective to better approximate formula (1). Third, PMFL incorporates the model-contrastive term with historical information into the local optimization function, thereby enhancing the model’s ability to adapt to data heterogeneity. Hence, these designs enable PMFL to achieve stable and high-accuracy performance under heterogeneous scenarios.

Notably, FedVarp and MIFA exhibit relatively weaker performance, particularly under the cyclic pattern. This is because they use the most recently submitted local updates from all nodes in each round. However, when node participation frequency is low, many nodes may fail to participate in training for multiple consecutive rounds. As a result, the cached updates for those nodes become stale, which slows down the convergence of the global model. Furthermore, FedHyper aggregates only the updates from currently participating nodes and employs a simple averaging strategy. Although FedHyper can adaptively adjust the local and global learning rates, its performance is significantly affected by participation heterogeneity. In contrast, FedAU dynamically adjusts aggregation weights based on each node’s cumulative participation count to correct the bias of the global optimization objective. Thus, it achieves stable performance across three participation patterns. However, since it does not address data heterogeneity, its overall performance remains inferior to that of our PMFL. Furthermore, FedPPO selects a subset of nodes to participate in the next round based on their estimated contributions. On SVHN and CIFAR10, its performance remains relatively stable across different participation patterns because these datasets are relatively simple and can converge even with few participating nodes. However, on CINIC and CIFAR100, FedPPO’s performance significantly deteriorates, indicating that contribution-based selection method cannot fundamentally resolve participation heterogeneity.

TABLE I
ACCURACY RESULTS (%) IN VARIOUS METHODS. THE BEST AND SECOND-BEST RESULTS ARE SHOWN IN BOLD AND UNDERLINED, RESPECTIVELY.

Participation pattern	Methods	SVHN		CIFAR10		CINIC		CIFAR100	
		Training	Test	Training	Test	Training	Test	Training	Test
Bernoulli	PMFL (ours)	88.03 (+1.00)	87.47 (+0.58)	86.99 (+0.97)	78.48 (+0.50)	68.49 (+1.15)	64.40 (+0.98)	54.16 (+1.43)	45.62 (+0.58)
	FedVarp [5]	85.73	85.45	83.06	77.83	60.47	58.77	49.73	42.82
	MIFA [6]	86.45	86.10	81.72	77.43	60.77	59.13	49.91	42.86
	FedHyper [46]	84.90	83.95	81.54	73.03	59.16	55.54	48.65	42.47
	FedAU [4]	<u>87.03</u>	<u>86.89</u>	<u>86.02</u>	<u>77.98</u>	<u>67.34</u>	<u>63.42</u>	<u>52.73</u>	<u>45.04</u>
	FedPPO [30]	86.95	86.61	85.85	77.92	65.64	62.35	50.80	43.63
Markovian	PMFL (ours)	88.56 (+0.92)	87.78 (+0.77)	86.79 (+0.82)	78.26 (+0.42)	67.99 (+1.12)	64.07 (+1.02)	52.18 (+1.51)	44.63 (+0.67)
	FedVarp [5]	86.73	86.25	82.52	77.24	61.09	59.26	49.45	42.64
	MIFA [6]	86.86	86.48	80.86	76.98	59.71	57.92	49.83	42.70
	FedHyper [46]	84.34	82.96	82.01	73.20	59.74	55.20	49.02	42.81
	FedAU [4]	<u>87.64</u>	<u>87.01</u>	<u>85.97</u>	<u>77.84</u>	<u>66.87</u>	<u>63.05</u>	<u>50.67</u>	<u>43.96</u>
	FedPPO [30]	86.25	85.84	84.47	77.40	61.25	58.79	49.86	42.63
Cyclic	PMFL (ours)	87.90 (+0.75)	87.55 (+0.50)	85.83 (+1.18)	77.90 (+0.87)	65.46 (+0.73)	61.89 (+0.48)	51.64 (+1.44)	43.99 (+0.43)
	FedVarp [5]	81.77	81.34	79.03	72.15	55.41	54.22	46.46	42.13
	MIFA [6]	76.13	75.65	69.50	67.57	60.77	59.12	45.08	41.86
	FedHyper [46]	84.89	83.81	80.80	72.62	59.16	55.54	48.87	42.70
	FedAU [4]	<u>87.15</u>	<u>87.05</u>	<u>84.65</u>	<u>77.03</u>	<u>64.73</u>	<u>61.41</u>	<u>50.20</u>	<u>43.56</u>
	FedPPO [30]	86.96	86.72	84.55	76.81	64.47	61.24	49.94	42.87

2) *Convergence of Different Methods:* To evaluate the convergence of different methods, we plot the training accuracy curves across multiple rounds for Bernoulli and Markovian patterns on SVHN, CIFAR10, and CINIC. The results for PMFL and the baseline methods are shown in Fig. 4. The results reveal that the training accuracy curves for FedVarp and MIFA exhibit extremely flat trajectories. This is because they incorporate the most recent updates from all nodes in each round, effectively implementing a “full participation” aggregation that produces smooth curves. In contrast, the training curves of FedPPO, FedHyper, and FedAU exhibit significant fluctuations, indicating unstable global model performance during training. This is because, under low participation rates, very few nodes actually participate in aggregation, making the global model’s performance more susceptible to fluctuations. Notably, PMFL’s training accuracy gradually stabilizes with increasing rounds, demonstrating its robustness under heterogeneous scenarios.

3) *The Impact of Data Heterogeneity for Different Methods:* To evaluate the performance of PMFL and the compared methods under varying degrees of data heterogeneity, we conduct experiments on SVHN. The data are split using a Dirichlet partition with concentration parameter $\alpha \in \{0.1, 0.3, 0.5, 0.8, 1.0, 2.0, 5.0\}$, where smaller α indicates higher data heterogeneity. The results are shown in Table II, where the best and second-best results highlighted in bold and underlined, respectively. We observe that as data heterogeneity increases (i.e., as α decrease), the performance of all methods generally declines, and this trend is consistent across different participation patterns. Notably, PMFL maintains high accuracy across all data heterogeneity conditions, which is attributed to its loss function that combines both classification term and model-contrastive term. This design minimizes local classification loss while enhancing the consistency of model updates across nodes, thereby mitigating the negative impact of data heterogeneity on the global model’s performance. Furthermore, we observe that MIFA performs poorly in the cyclic pattern, regardless of the degree of data heterogeneity.

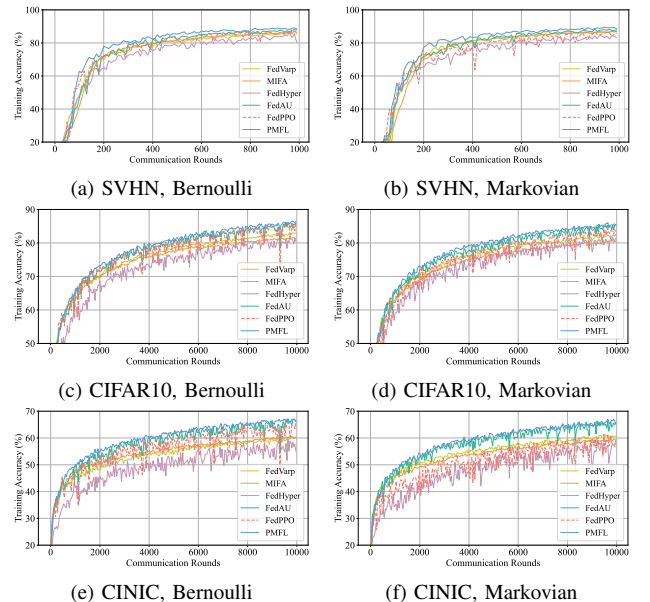


Fig. 4. Training accuracy of PMFL and the compared methods across different training rounds.

This is because each node alternates between participation and non-participation in fixed cycles, which leads to delayed historical model updates. In summary, the results show that PMFL is more robust than the compared methods under diverse data heterogeneity settings.

4) *Effects of Participation Heterogeneity Across Methods:* To evaluate the performance of PMFL and the compared methods under varying levels of participation heterogeneity, we conduct experiments on CIFAR10. The participation heterogeneity is controlled by the parameter $\beta \in \{0.01, 0.05, 0.1, 0.5, 1.0, 2.0, 5.0\}$, where smaller β indicates higher heterogeneity. All experiments follow the Bernoulli pattern. The results are shown in Table III. Similar to the trend of data heterogeneity in Table II, the performance of all methods generally degrades with increasing heterogeneity. In all methods, PMFL demonstrates the best performance. Fur-

TABLE II
ACCURACY RESULTS (%) IN VARIOUS METHODS WITH DIFFERENT DATA HETEROGENEITY ON SVHN.

Participation pattern	Methods	$\alpha = 0.1$		$\alpha = 0.3$		$\alpha = 0.5$		$\alpha = 0.8$		$\alpha = 1.0$		$\alpha = 2.0$		$\alpha_p = 5.0$	
		Training	Test	Training	Test	Training	Test	Training	Test	Training	Test	Training	Test	Training	Test
Bernoulli	PMFL (ours)	88.03	87.47	90.40	89.88	91.68	90.95	91.82	91.16	91.37	90.65	92.51	91.60	91.79	91.15
	FedVarp [5]	85.72	85.45	89.06	88.69	90.26	89.63	89.96	89.42	89.93	89.34	90.98	90.12	90.71	90.27
	MIFA [6]	86.45	86.09	88.68	88.00	89.83	89.24	89.65	88.94	89.18	88.74	90.57	89.62	90.31	89.84
	FedHyper [46]	84.90	83.95	89.19	88.81	89.71	89.30	90.74	90.02	90.36	89.74	91.31	90.45	91.17	90.64
	FedAU [4]	<u>87.03</u>	<u>86.89</u>	<u>89.82</u>	<u>89.43</u>	<u>90.59</u>	<u>90.09</u>	<u>90.88</u>	<u>90.56</u>	<u>90.76</u>	<u>90.23</u>	<u>91.71</u>	<u>90.92</u>	<u>91.46</u>	<u>90.76</u>
	FedPPO [30]	86.95	86.61	89.34	89.11	89.46	89.43	90.18	89.50	<u>90.86</u>	<u>90.34</u>	91.17	90.47	91.41	90.70
Markovian	PMFL (ours)	88.56	87.78	90.53	90.08	91.95	91.66	91.97	91.32	91.43	90.56	92.53	91.71	92.04	91.48
	FedVarp [5]	86.73	86.25	88.96	88.50	89.49	88.78	89.56	89.12	89.99	89.48	90.79	90.12	90.42	89.90
	MIFA [6]	86.86	86.48	88.34	87.97	89.19	88.54	88.77	88.35	88.63	88.15	90.48	89.71	89.39	88.87
	FedHyper [46]	84.34	82.96	88.85	88.17	89.92	89.32	90.25	89.87	<u>90.67</u>	<u>90.17</u>	90.88	90.26	91.36	90.91
	FedAU [4]	<u>87.64</u>	<u>87.01</u>	<u>90.17</u>	<u>89.56</u>	<u>90.82</u>	<u>90.48</u>	<u>91.20</u>	<u>90.59</u>	<u>90.66</u>	<u>90.04</u>	<u>91.67</u>	<u>90.99</u>	<u>91.46</u>	<u>90.83</u>
	FedPPO [30]	86.25	85.84	89.55	88.83	90.07	89.72	90.75	89.79	90.40	90.07	90.99	90.10	91.38	90.52
Cyclic	PMFL (ours)	87.90	87.55	90.63	89.81	91.30	90.57	91.83	91.00	91.10	90.67	92.28	91.43	91.66	91.01
	FedVarp [5]	81.77	81.34	85.91	85.39	87.62	87.03	86.94	86.57	86.51	85.89	88.70	88.46	87.76	87.42
	MIFA [6]	76.13	75.65	77.75	77.47	86.23	85.77	84.90	84.17	76.63	76.35	87.66	87.54	83.35	82.78
	FedHyper [46]	84.89	83.81	89.03	88.41	90.30	89.73	89.89	89.12	89.90	89.41	90.65	89.97	90.85	90.38
	FedAU [4]	<u>87.15</u>	<u>87.05</u>	<u>89.94</u>	<u>89.30</u>	<u>90.72</u>	<u>90.15</u>	<u>91.07</u>	<u>90.55</u>	<u>90.41</u>	<u>89.98</u>	<u>91.38</u>	<u>90.79</u>	<u>91.25</u>	<u>90.56</u>
	FedPPO [30]	86.96	86.72	89.68	89.25	90.89	90.13	90.92	90.34	<u>90.75</u>	<u>90.34</u>	<u>91.71</u>	<u>90.86</u>	91.73	91.14

TABLE III
ACCURACY RESULTS (%) IN VARIOUS METHODS ON CIFAR10 WITH DIFFERENT BERNOULLI PARTICIPATION HETEROGENEITY.

Methods	$\beta = 0.01$		$\beta = 0.05$		$\beta = 0.1$		$\beta = 0.5$		$\beta = 1.0$		$\beta = 2.0$		$\beta = 5.0$	
	Training	Test	Training	Test	Training	Test	Training	Test	Training	Test	Training	Test	Train	Test
PMFL (ours)	86.37	78.08	86.25	78.15	86.99	78.48	89.62	78.80	89.46	79.25	89.72	79.48	90.00	79.21
FedVarp [5]	78.90	74.88	82.06	77.12	83.06	77.83	83.13	76.78	84.41	77.96	86.25	78.20	84.51	77.58
MIFA [6]	80.14	76.16	81.00	77.25	81.72	77.43	82.94	76.89	83.66	77.50	83.86	77.31	83.98	77.36
FedHyper [46]	76.69	69.34	78.89	71.18	81.54	73.03	84.66	76.27	84.72	76.81	86.77	77.80	87.03	78.39
FedAU [4]	<u>85.19</u>	<u>77.30</u>	<u>85.74</u>	<u>77.44</u>	<u>86.02</u>	<u>77.98</u>	<u>88.53</u>	<u>78.44</u>	<u>87.98</u>	<u>78.56</u>	88.50	<u>78.66</u>	<u>88.67</u>	78.26
FedPPO [30]	84.38	77.26	85.40	<u>77.48</u>	85.85	77.02	86.76	78.04	87.02	78.28	<u>88.56</u>	78.62	87.76	<u>78.62</u>

thermore, under high participation heterogeneity (i.e., smaller β values), the accuracy of MIFA and FedVarp outperforms that of FedHyper. However, as β increases, their performance gradually drops below that of FedHyper. This phenomenon is due to MIFA and FedVarp both caching the last model update from each node for aggregation. When participation heterogeneity is high (i.e., smaller β), the server uses the last model update from each node to compute the global model, which mitigates the impact of participation heterogeneity. In contrast, when node participation becomes uniform (i.e., larger β), participation heterogeneity is alleviated. In this case, MIFA and FedVarp may aggregate stale last-submitted updates, which slows the convergence of the global model.

5) *Node-wise Distributions of Loss and Accuracy*: To visualize the differences of the global model performance across nodes in PMFL, we plot the Cumulative Distribution Functions (CDF) curves for accuracy and loss, and compare them with those of FedVarp. The CDF describes the proportion of samples whose values are less than or equal to a given threshold, and thus reflects the distribution of a metric (e.g., accuracy or loss). In the experiments, we evaluate the training accuracy and training loss of the trained global model at each node on SVHN and plot the CDF curves of these values, as shown in Fig. 5. Notably, the global model is trained under the Bernoulli pattern. We observe that, for PMFL, most nodes achieve training accuracy between 80% and 100%, and their training loss values are largely concentrated below 0.05. In contrast, FedVarp exhibits a more dispersed distribution for both training accuracy and training loss. These results indicate that PMFL achieves more consistent model performance across nodes under heterogeneous conditions.

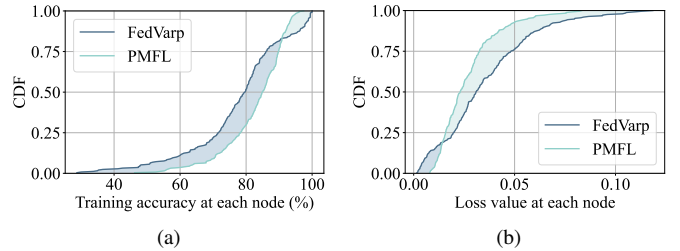


Fig. 5. Node-wise distributions of training accuracy and loss value on SVHN with Bernoulli participation.

6) *Node Aggregation Weights in PMFL*: To explore the variation of node aggregation weights in PMFL, we plot the curve of node aggregation weights across communication rounds. In the experiments, we use the CIFAR10 under the Bernoulli pattern, with all parameters set to their default values. As shown in Fig. 6(a), we observe that the average aggregation weight across all nodes is approximately 22. As shown in Fig. 6(b), when a node has a high participation frequency (e.g., 40.2%), its aggregation weight stays above 2.8. Conversely, when the node participation frequency is low (i.e., 2%), as shown in Fig. 6(c), its aggregation weight remains above 30. This dynamic adjustment of aggregation weights effectively prevents the global model from being biased towards nodes with higher participation frequency. These results validate that PMFL can automatically adjust aggregation weights according to each node's average participation interval.

7) *The Choice of Different Cutoff Interval C on PMFL*: The cutoff interval C affects each node's aggregation weight, and thus influences the performance of PMFL. To evaluate

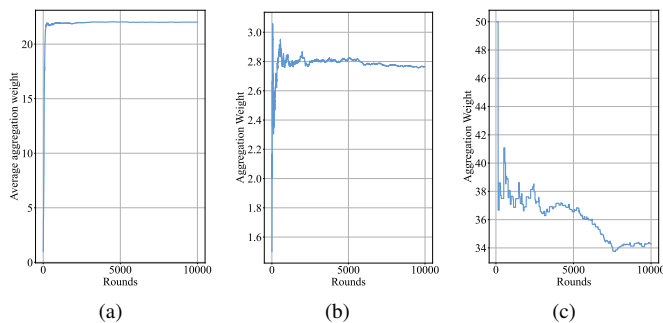


Fig. 6. Aggregation weights with Bernoulli participation, (a) average aggregation weights over all nodes, (b) aggregation weights of a single node with a high participation frequency of 40.2%, (c) aggregation weights of a single node with a low participation frequency of 2%.

TABLE IV
ACCURACY (%) ON TRAINING AND TEST DATA OF PMFL ON SVHN,
WITH DIFFERENT CUTOFF INTERVALS C .

Participation pattern	C	$\beta = 0.1$		$\beta = 0.2$		$\beta = 0.4$	
		Training	Test	Training	Test	Training	Test
Bernoulli	20	87.74	87.16	87.89	87.19	88.36	87.93
	50	88.03	87.47	<u>87.82</u>	<u>87.08</u>	88.87	88.37
	100	87.22	86.51	85.48	84.52	87.85	87.59
	200	84.56	83.84	84.18	83.70	87.29	87.11
Markovian	20	87.83	87.20	87.64	87.01	<u>88.53</u>	<u>88.28</u>
	50	88.56	87.78	88.41	87.67	89.53	88.95
	100	87.02	86.36	85.92	85.74	88.22	87.67
	200	84.87	84.45	85.17	84.58	88.34	87.89
Cyclic	20	<u>87.52</u>	<u>87.02</u>	<u>84.24</u>	<u>83.83</u>	<u>87.35</u>	<u>87.14</u>
	50	87.90	87.55	87.16	86.46	87.62	87.46
	100	85.22	84.76	84.55	84.01	87.16	86.21
	200	81.37	80.62	81.06	80.30	86.81	85.74

the impact of C , we set $C \in \{20, 50, 100, 200\}$ to evaluate the performance of PMFL on the SVHN under different participation patterns. All other parameters are set to their default values. For each subtable, the best and second-best results are highlighted in bold and underlined, respectively. The results are reported in Table IV. We observe that when $C=200$, the performance of PMFL decreases significantly. This is because an excessively large C amplifies the aggregation weights of nodes that have not participated in training for many rounds, thereby hindering the convergence of the global model. Conversely, if C is set too small, it may distort the actual participation frequencies of nodes, causing the optimization to deviate from the intended FL objective. These results indicate that PMFL requires a properly cutoff interval C . We notice that the global model achieves the best performance when $C=50$, which is considered an appropriate setting.

8) *Ablation Study about PMFL*: By incorporating the model-contrastive term in local model training, designing the adaptive aggregation weight calculation step and introducing historical information in during the aggregation phase, PMFL improves FL performance in heterogeneous environments. To evaluate the contributions of each component in PMFL, we conduct an ablation study. Specifically, we evaluate PMFL on the CIFAR10 under the bernoulli pattern. The results are reported in Table V, where “w/o” denotes “without”. We observe that removing the MCT (i.e., the model-contrastive term) reduces the test accuracy of the global model. This is because, without the model-contrastive term, local training relies solely on the classification term, which exacerbates

TABLE V
IMPACT OF EACH COMPONENT IN PMFL UNDER CIFAR10 DATASET.

Methods	Data Distribution	Test Accuracy (%)			
		$\beta = 0.01$	$\beta = 0.05$	$\beta = 0.10$	$\beta = 0.50$
PMFL	$\alpha = 0.5$	79.04	79.27	79.49	79.73
	$\alpha = 0.1$	78.08	78.15	78.48	78.80
w/o MCT	$\alpha = 0.5$	78.94	79.06	79.23	79.45
	$\alpha = 0.1$	77.63	77.81	78.26	78.49
w/o AWC	$\alpha = 0.5$	71.86	73.05	75.07	75.80
	$\alpha = 0.1$	69.72	72.18	74.72	75.35
w/o HGM	$\alpha = 0.5$	79.13	79.24	79.39	79.96
	$\alpha = 0.1$	77.61	77.73	77.96	78.25

Note: “MCT” represents the model-contrastive term, “AWC” denotes the adaptive aggregation weight calculation step, and “HGM” denotes the historical global models. Best results are in **bold**.

inconsistency among model updates. Moreover, under different heterogeneous conditions, PMFL’s performance degrades significantly when AWC is removed. This is because the global optimization objective of FL shifts toward the local optimization objectives of nodes with higher participation frequency. Notably, when the data heterogeneity is $\alpha=0.5$, removing HGM (i.e., historical global models) has only a minor impact on PMFL’s test accuracy. However, when $\alpha=0.1$, removing HGM decreases the test accuracy by more than 0.5% compared with PMFL. This indicates that integrating historical global models is particularly beneficial under highly heterogeneous data distributions. In summary, the results show that each component in PMFL contributes positively to improving the performance of FL in heterogeneous scenarios.

9) *Consistency of PMFL in Non-IID Settings*: The designed model-contrastive term promotes the alignment between local and global models, thereby improving the consistency of model updates across nodes. To assess this improvement in consistency, we measure the deviation among model updates, which is defined as follows.

Definition 1. (*Deviation*) Given that in the t -th round, each node $k \in \mathcal{K}^t$ submits its model update Δ_k^t , the deviation among model updates is given by:

$$\text{Dev}^t = \sum_{k \in \mathcal{K}^t} (1 - \text{Sim}(\Delta_k^t, \bar{\Delta}^t)),$$

where $\text{Sim}(\cdot)$ is the cosine similarity between two vectors, and Dev^t measures the deviation among model updates.

Remark 1. If all $k_1, k_2 \in \mathcal{K}^t$ satisfy $\Delta_{k_1}^t = \Delta_{k_2}^t$, then the relation $\bar{\Delta}^t = \Delta_k^t$ holds. In this case, the model updates are perfectly consistent, which implies $\text{Dev}^t = 0$. Conversely, a larger Dev^t reflects significant inconsistency among updates.

According to Definition 1, we measure the deviation among nodes’ model updates in PMFL. For comparison, we evaluate an ablated PMFL variant without the model-contrastive term in the local objective (w/o MCT). Experiments are conducted on CIFAR10 under bernoulli pattern, and the results are reported in Fig. 7. We observe that PMFL achieves a lower deviation than w/o MCT. This reduction is mainly attributed to the model-contrastive term incorporated into PMFL’s local objective, which strengthens the alignment between local and global models and thereby improves the consistency of model updates across nodes. These results demonstrate the effectiveness of the proposed model-contrastive term.

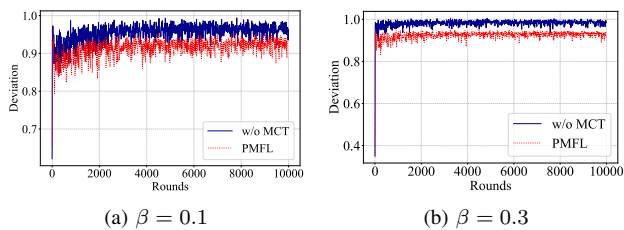


Fig. 7. Deviation of PMFL under varying participation heterogeneity levels.

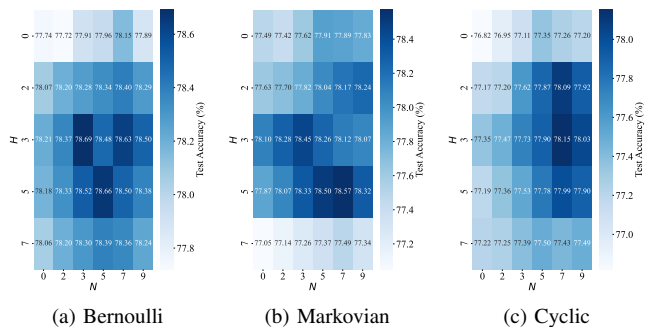


Fig. 8. Accuracy results of PMFL under local and global sliding buffer sizes on the CIFAR10.

10) Impact of Local and Global Sliding Buffer on PMFL: Each node in PMFL maintains a local sliding buffer to store its historical local models, thereby providing more positive and negative samples. Meanwhile, during the aggregation phase, the server introduces a global sliding buffer to store historical global models, enabling the updated global model to integrate information from previous rounds. To evaluate the sensitivity of PMFL to the local buffer size N and global buffer size H , we conduct experiments on the CIFAR10, where H is selected from the range $\{0, 2, 3, 5, 7, 9\}$, and N is selected from $\{0, 2, 3, 5, 7\}$, with other parameters kept at their default values. The results are shown in Fig. 8. We observe that when $H > 0$, PMFL outperforms the $H = 0$ setting across all participation patterns, indicating that integrating historical global models into aggregation improves FL performance in heterogeneous scenarios. However, when the global buffer size increases to $H = 7$, the performance begins to decline. Although a larger global buffer allows more historical global models to contribute to the latest global model, stale information may interfere with the optimization process, hindering the FL convergence. These results suggest that integrating historical global models is beneficial, but overreliance on outdated global models may degrade performance. Additionally, we observe that increasing the local buffer size enhances the performance of the global model. A larger local buffer provides more positive and negative samples for computing the model-contrastive loss, which strengthens the effectiveness of the model-contrastive term. Thus, properly configuring both local and global buffers plays a positive role in boosting the performance of PMFL.

11) Global Model Performance Fluctuations of PMFL: In PMFL, the historical global models are incorporated into the aggregation phase to mitigate performance fluctuations of the global model across adjacent rounds. To evaluate its effectiveness, we conduct experiments on the CIFAR10 under the

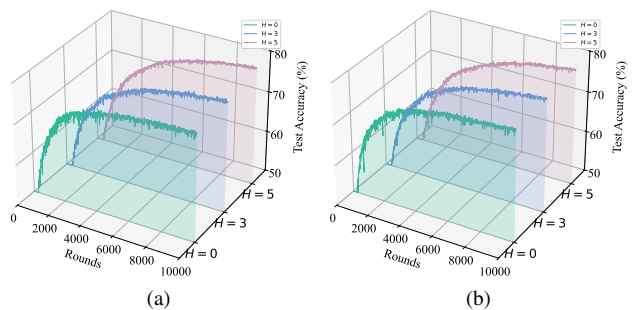


Fig. 9. Test accuracy of the global model in MCFL over rounds under different expected participation frequencies $\mathbb{E}[p_k]$. (a) $\mathbb{E}[p_k]=0.05$, (b) $\mathbb{E}[p_k]=0.10$.

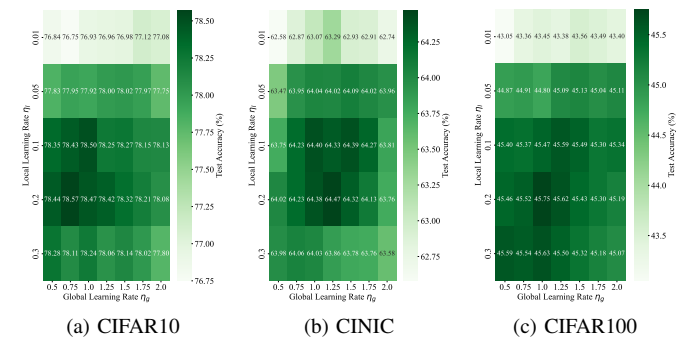


Fig. 10. Test accuracy of PMFL with varying learning rates η_l and η_g .

bernoulli pattern. The expected participation frequency $\mathbb{E}[p_k]$ is set to 0.05 and 0.10, respectively, and the global sliding buffer size H is set to 0, 3, and 5. The results are shown in Fig. 9. We observe that the global model’s test accuracy exhibits the largest fluctuations when when $H = 0$. As the global sliding buffer size increases, the fluctuations gradually diminish. This indicates that PMFL effectively mitigates the instability of the global model under low participation rates by integrating historical global models. This facilitates more stable global representations for model-contrastive term. However, Fig. 8 shows that an overly large global buffer degrades the global model’s performance. This is because incorporating too many historical models amplifies the smoothing effect, causing the global updates to rely excessively on outdated information.

12) Impact of Learning Rates η_l and η_g on PMFL: Different local learning rates η_l and global learning rates η_g can affect the performance of FL. To evaluate the sensitivity of PMFL under different learning rate configurations, we conduct experiments on the CIFAR10, CINIC, and CIFAR100 under the Bernoulli pattern. Specifically, the global learning rate is selected from $\{0.5, 0.75, 1, 1.25, 1.5, 1.75, 2.0\}$, while the local learning rate is chosen from $\{0.01, 0.05, 0.1, 0.2, 0.3\}$. The test accuracy results are presented in Fig. 10, where deeper green indicates higher accuracy. The results show that different local learning rate settings lead to accuracy variations of 0%-2%, with PMFL achieving the lowest performance when the local learning rate is set to 0.01. This is because, under a limited number of rounds, smaller local learning rates reduce the magnitude of model updates, thereby slowing model convergence. In addition, we observe that changes in the global learning rate have a relatively small impact on performance. This is because PMFL’s global update depends

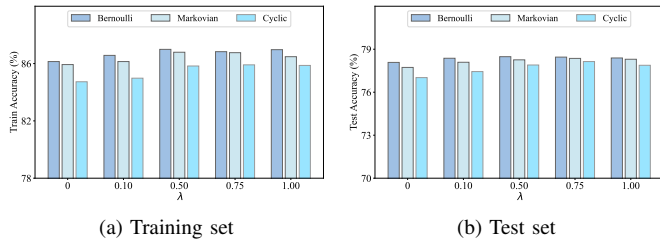


Fig. 11. Accuracy results with varying importance coefficients λ in PMFL.

primarily on the model updates uploaded by the nodes, whose update magnitudes are mainly determined by the local learning rate. Overall, these results indicate that PMFL exhibits low sensitivity to both local and global learning rate settings.

13) Impact of Model-Contrastive Term on PMFL: To evaluate the impact of the importance coefficient λ of the model-contrastive term on PMFL, we conduct experiments on CIFAR10 under three participation patterns, with $\lambda \in \{0, 0.10, 0.50, 0.75, 1.00\}$. Fig. 11 reports the performance of PMFL under different λ values. The results show that when $\lambda=0$, PMFL achieves the worst performance across all participation patterns. This is because setting $\lambda=0$ removes the model-contrastive term from the optimization function, weakening the consistency among model updates across nodes and degrading FL performance under data heterogeneity. As λ increases, the performance of PMFL gradually improves, indicating that the model-contrastive term improves FL performance in heterogeneous data settings. However, as λ increases to 0.75 and 1.00, the performance of the PMFL reaches a stable state. This is because the performance gain provided by the model-contrastive term is limited. They do not continue to increase with larger values of λ . Moreover, an excessively large λ may cause “over-alignment” between local and global model representations, thereby restricting the model’s classification performance. Thus, the importance coefficient λ should not be set excessively large.

14) Stability of PMFL: To evaluate the robustness of PMFL, it is essential to examine its stability across repeated experiments. To this end, we conduct experiments on CIFAR10 and CINIC, using three participation patterns. Specifically, for each experimental setting, we repeat the experiment 10 times. We record the test accuracy of the global model at the final round of each run and use these values to assess the stability of PMFL. The test accuracy results are shown in the Fig. 12. It can be observed that the performance variation of PMFL on both CIFAR10 and CINIC is within 0.5%, indicating that PMFL maintains consistent results under different participation scenarios. Notably, no outliers are observed in these experiments, which further validates the stability of PMFL.

15) Scalability of PMFL: In practical FL scenarios, the total number of nodes is uncertain. To evaluate the scalability of PMFL, we test its performance with different numbers of nodes. Specifically, we set the total number of nodes in the FL system to $K \in \{200, 220, 240, 250, 260, 280, 300\}$. The experiments are conducted under Bernoulli and Markovian patterns. The results are shown in Fig. 13. It can be observed that the test accuracy of PMFL decreases slightly as the

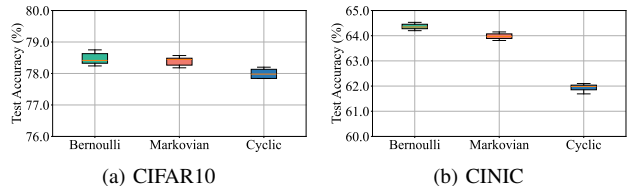


Fig. 12. Stability of test accuracy of PMFL on CIFAR10 and CINIC under different participation patterns.

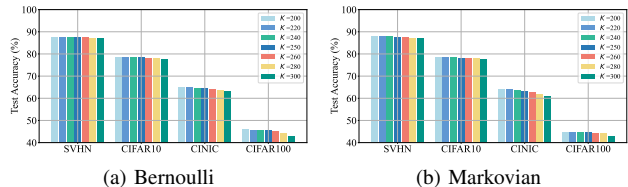


Fig. 13. Test accuracy of PMFL on SVHN, CIFAR10, CINIC, and CIFAR100 with different numbers of nodes.

number of nodes gradually increases. This phenomenon stems from the increased uncertainty in local data distributions and participation frequencies caused by the expansion of system nodes, which slightly impacts PMFL’s learning performance. Overall, PMFL maintains stable accuracy across all configurations, highlighting its scalability.

16) Time Cost: To evaluate the time cost of PMFL, we measure its training time and aggregation time. Specifically, we compare the per-round training time of PMFL with that of PMFL (w/o MCT), where PMFL (w/o MCT) denotes a variant of PMFL whose local function is defined without the model-contrastive term. All experiments are conducted on an NVIDIA A800 GPU. The training times of PMFL (w/o MCT) and PMFL on the CIFAR10 are presented in Fig. 14(a). It can be observed that, PMFL (w/o MCT) exhibits a shorter training time than PMFL, regardless of the number of local iterations. This is because PMFL incorporates the model-contrastive term into its optimization function, resulting in additional computational cost. Moreover, we compare the aggregation time of PMFL with that of compared methods within a single communication round, as shown in Fig. 14(b). We notice that FedVarp and MIFA take the longest time to aggregate because they aggregate model updates from all nodes, including both participating nodes and non-participating nodes. Moreover, we observe that FedHyper and FedPPO achieve the shortest aggregation time since they operate only on the model updates of currently participating nodes. Compared with these methods, PMFL take a slightly higher aggregation cost because the server computes aggregation weights for each node and incorporates historical global models. Since PMFL improves the global model performance under heterogeneous scenarios, this additional time cost remains within an acceptable range.

VII. CONCLUSION

In this paper, we propose PMFL, a performance-enhanced model-contrastive federated learning framework that improves the FL performance in heterogeneous scenarios. PMFL leverages historical local models into the model-contrastive term of the optimization function to construct stable contrastive points,

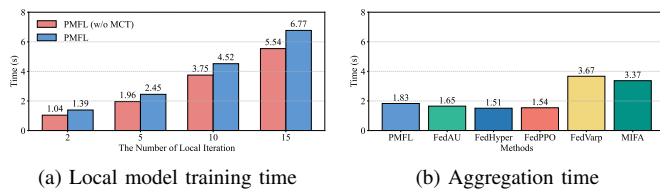


Fig. 14. Time cost of different methods in SVHN dataset.

thereby enhancing the effectiveness of model-contrastive term. Moreover, PMFL employs the aggregation strategy that adaptively adjusts aggregation weights and incorporates historical global models. Extensive experiments validate the effectiveness and superiority of PMFL compared to other methods under heterogeneous scenarios. For future work, we plan to investigate model heterogeneity in FL.

REFERENCES

- [1] B. McMahan, E. Moore, D. Ramage, S. Hampson, and B. A. y Arcas, "Communication-efficient learning of deep networks from decentralized data," in *Proc. Artif. Intell. Statist.*, 2017, pp. 1273–1282.
- [2] Z. Lu, H. Pan, Y. Dai, X. Si, and Y. Zhang, "Federated learning with non-iid data: A survey," *IEEE Internet Things J.*, vol. 11, no. 11, pp. 19 188–19 209, 2024.
- [3] X. Zhang, J. Li, R. Yin, and W. Wang, "Fednk-rf: Federated kernel learning with heterogeneous data and optimal rates," *IEEE Trans. Neural Netw. Learn. Syst.*, pp. 1–13, 2025.
- [4] S. Wang and M. Ji, "A lightweight method for tackling unknown participation statistics in federated averaging," in *Proc. Int. Conf. Learn. Representations*, 2024.
- [5] D. Jhunjhunwala, P. Sharma, A. Nagarkatti, and G. Joshi, "Fedvarp: Tackling the variance due to partial client participation in federated learning," in *Proc. Uncertainty Artif. Intell.*, 2022, pp. 906–916.
- [6] X. Gu, K. Huang, J. Zhang, and L. Huang, "Fast federated learning in the presence of arbitrary device unavailability," in *Proc. Adv. Neural Inf. Process. Syst.*, vol. 34, 2021, pp. 12 052–12 064.
- [7] A. M. Albaseer, M. Abdallah, A. Al-Fuqaha, A. M. Seid, A. Erbad, and O. A. Dobre, "Fair selection of edge nodes to participate in clustered federated multitask learning," *IEEE Trans. Netw. Serv. Manage.*, vol. 20, no. 2, pp. 1502–1516, 2023.
- [8] K. Yang, S. Chen, and C. Shen, "On the convergence of hybrid server-clients collaborative training," *IEEE J. Sel. Areas Commun.*, vol. 41, no. 3, pp. 802–819, 2023.
- [9] A. Albaseer, M. Abdallah, A. Al-Fuqaha, and A. Erbad, "Data-driven participant selection and bandwidth allocation for heterogeneous federated edge learning," *IEEE Trans. Syst., Man, Cybern. Syst.*, vol. 53, no. 9, pp. 5848–5860, 2023.
- [10] L. Luo, C. Zhang, H. Yu, G. Sun, S. Luo, and S. Dustdar, "Communication-efficient federated learning with adaptive aggregation for heterogeneous client-edge-cloud network," *IEEE Trans. Serv. Comput.*, vol. 17, no. 6, pp. 3241–3255, 2024.
- [11] A. Krizhevsky, G. Hinton *et al.*, "Learning multiple layers of features from tiny images," 2009. [Online]. Available: <http://www.cs.utoronto.ca/~kriz/learning-features-2009-TR.pdf>
- [12] Q. Li, B. He, and D. Song, "Model-contrastive federated learning," in *Proc. IEEE/CVF Conf. Comput. Vis. Pattern Recognit.*, 2021, pp. 10 713–10 722.
- [13] H. Zhang *et al.*, "Towards model-contrastive federated learning with lightweight privacy preservation and poisoning attack detection," *IEEE Trans. Dependable Secure Comput.*, pp. 1–17, 2025.
- [14] Y. Miao, W. Zheng, X. Li, H. Li, K. R. Choo, and R. H. Deng, "Secure model-contrastive federated learning with improved compressive sensing," *IEEE Trans. Inf. Forensics Security*, vol. 18, pp. 3430–3444, 2023.
- [15] S. Seo, J. Kim, G. Kim, and B. Han, "Relaxed contrastive learning for federated learning," in *Proc. IEEE/CVF Conf. Comput. Vis. Pattern Recognit.*, 2024, pp. 12 279–12 288.
- [16] Y. Yang, X. Liu, T. Gao, X. Xu, P. Zhang, and G. Wang, "Dense contrastive-based federated learning for dense prediction tasks on medical images," *IEEE Journal of Biomedical and Health Informatics*, vol. 28, no. 4, pp. 2055–2066, 2024.
- [17] T. Zhou, J. Zhang, and D. H. K. Tsang, "Fedfa: Federated learning with feature anchors to align features and classifiers for heterogeneous data," *IEEE Trans. Mobile Comput.*, vol. 23, no. 6, pp. 6731–6742, 2024.
- [18] P. Khosla *et al.*, "Supervised contrastive learning," in *Proc. Adv. Neural Inf. Process. Syst.*, vol. 33, 2020, pp. 18 661–18 673.
- [19] J. Wang, Q. Liu, H. Liang, G. Joshi, and H. V. Poor, "Tackling the objective inconsistency problem in heterogeneous federated optimization," in *Proc. Adv. Neural Inf. Process. Syst.*, vol. 33, 2020, pp. 7611–7623.
- [20] Y. Deng *et al.*, "Improving federated learning with quality-aware user incentive and auto-weighted model aggregation," *IEEE Trans. Parallel Distrib. Syst.*, vol. 33, no. 12, pp. 4515–4529, 2022.
- [21] Z. Li, T. Lin, X. Shang, and C. Wu, "Revisiting weighted aggregation in federated learning with neural networks," in *Proc. Int. Conf. Mach. Learn.*, vol. 202, 2023, pp. 19 767–19 788.
- [22] S. Chen, C. Shen, L. Zhang, and Y. Tang, "Dynamic aggregation for heterogeneous quantization in federated learning," *IEEE Trans. Wireless Commun.*, vol. 20, no. 10, pp. 6804–6819, 2021.
- [23] X. Li, Y. Gao, Y. Deng, and X. Jiang, "Federated learning with adaptive aggregation weights for non-iid data in edge networks," *IEEE Trans. Cognit. Commun. Networking*, pp. 1–1, 2025.
- [24] H.-R. Zhang, R. Chen, S.-H. Wen, and X.-Q. Bian, "Swim: Sliding-window model contrast for federated learning," *Future Gener. Comput. Syst.*, vol. 164, no. 107590, 2025.
- [25] B. Xu *et al.*, "Heterogeneous federated learning driven by multi-knowledge distillation," *IEEE Trans. Mobile Comput.*, pp. 1–14, 2025.
- [26] W. Ning *et al.*, "One teacher is enough: A server-clueless federated learning with knowledge distillation," *IEEE Trans. Serv. Comput.*, vol. 17, no. 5, pp. 2704–2718, 2024.
- [27] G. Liao, B. Luo, Y. Feng, M. Zhang, and X. Chen, "Optimal mechanism design for heterogeneous client sampling in federated learning," *IEEE Trans. Mobile Comput.*, vol. 23, no. 11, pp. 10 598–10 609, 2024.
- [28] B. Luo, W. Xiao, S. Wang, J. Huang, and L. Tassiulas, "Adaptive heterogeneous client sampling for federated learning over wireless networks," *IEEE Trans. Mobile Comput.*, vol. 23, no. 10, pp. 9663–9677, 2024.
- [29] H. Xu, J. Li, W. Wu, and H. Ren, "Federated learning with sample-level client drift mitigation," in *Proc. AAAI Conf. Artif. Intell.*, vol. 39, no. 20, 2025, pp. 21 752–21 760.
- [30] Z. Zhao, A. Li, R. Li, L. Yang, and X. Xu, "Fedppo: Reinforcement learning-based client selection for federated learning with heterogeneous data," *IEEE Trans. Cognit. Commun. Networking.*, vol. 11, no. 6, pp. 4141–4153, 2025.
- [31] H. Huang, W. Shi, Y. Feng, C. Niu, G. Cheng, J. Huang, and Z. Liu, "Active client selection for clustered federated learning," *IEEE Trans. Neural Netw. Learn. Syst.*, vol. 35, no. 11, pp. 16 424–16 438, 2024.
- [32] Z. Wu, Z. Xu, D. Zeng, Q. Wang, and J. Liu, "Advocating for the silent: Enhancing federated generalization for nonparticipating clients," *IEEE Trans. Neural Netw. Learn. Syst.*, vol. 36, no. 8, pp. 14 174–14 188, 2025.
- [33] K. Bonawitz *et al.*, "Towards federated learning at scale: System design," *Proc. Mach. Learn. Syst.*, vol. 1, pp. 374–388, 2019.
- [34] B. Ying, Z. Li, and H. Yang, "Exact and linear convergence for federated learning under arbitrary client participation is attainable," 2025. [Online]. Available: <https://arxiv.org/abs/2503.20117>
- [35] M. Xiang, S. Ioannidis, E. Yeh, C. Joe-Wong, and L. Su, "Efficient federated learning against heterogeneous and non-stationary client unavailability," in *Proc. Adv. Neural Inf. Process. Syst.*, vol. 37, 2024, pp. 104 281–104 328.
- [36] S. Weng, C. Ren, M. Xiao, and M. Skoglund, "Heterogeneity-aware client sampling: A unified solution for consistent federated learning," 2025. [Online]. Available: <https://arxiv.org/abs/2505.11304>
- [37] X. Liu *et al.*, "Self-supervised learning: Generative or contrastive," *IEEE Trans. Knowl. Data Eng.*, vol. 35, no. 1, pp. 857–876, 2021.
- [38] L. Zheng, B. Jing, Z. Li, H. Tong, and J. He, "Heterogeneous contrastive learning for foundation models and beyond," in *Proc. ACM Conf. Knowl. Discov. Data Mining*, 2024, pp. 6666–6676.
- [39] J. Gu *et al.*, "Recent advances in convolutional neural networks," *Pattern Recognit.*, vol. 77, pp. 354–377, 2018.
- [40] K. Zhang, M. Sun, T. X. Han, X. Yuan, L. Guo, and T. Liu, "Residual networks of residual networks: Multilevel residual networks," *IEEE Trans. Circuits Syst. Video Technol.*, vol. 28, no. 6, pp. 1303–1314, 2017.
- [41] Y. Netzer *et al.*, "Reading digits in natural images with unsupervised feature learning," in *Proc. Int. Conf. Neural Inf. Process. Syst. Workshop*, 2011.
- [42] L. N. Darlow, E. J. Crowley, A. Antoniou, and A. J. Storkey, "Cinic-10 is not imagenet or cifar-10," *arXiv preprint arXiv:1810.03505*, 2018.

- [43] X. Mu *et al.*, “Feddmc: Efficient and robust federated learning via detecting malicious clients,” *IEEE Trans. Dependable Secure Comput.*, vol. 21, no. 6, pp. 5259–5274, 2024.
- [44] X. Zhang *et al.*, “Fltracer: Accurate poisoning attack provenance in federated learning,” *IEEE Trans. Inf. Forensics Security*, vol. 19, pp. 9534–9549, 2024.
- [45] J. Lin, “On the dirichlet distribution,” *Master’s thesis, Dept. Math. Statist., Queen’s Univ.*, vol. 40, 2016.
- [46] Z. Wang, J. Wang, and A. Li, “Fedhyper: A universal and robust learning rate scheduler for federated learning with hypergradient descent,” in *Proc. Int. Conf. Learn. Representations*, 2024.